Study of filamentation with a high power high repetition rate ps laser at 1.03 μm

Aurélien Houard, Vytautas Jukna, Guillaume Point, Yves-Bernard André, S Klingebiel, M Schultze, Knut Michel, Thomas Metzger, André Mysyrowicz

Study of filamentation with a high power high repetition rate ps laser at 1.03 µm

A. Houard,[1,*] V. Jukna,[1] G. Point,[1] Y-B. André,[1] S. Klingebiel,[2] M. Schultze,[2] K. Michel,[2] T. Metzger,[2] and A. Mysyrowicz[1]

[1]LOA, ENSTA ParisTech, CNRS, Ecole polytechnique, Université Paris-Saclay, 828 bd des Maréchaux, 91762 Palaiseau cedex France

[2]TRUMPF Scientific Lasers GmbH + Co. KG, Feringastr. 10a, 85774, Unterföhring, Germany

[*]aurelien.houard@ensta-paristech.fr

Abstract: We study the propagation of intense, high repetition rate laser pulses of picosecond duration at 1.03 µm central wavelength through air. Evidence of filamentation is obtained from measurements of the beam profile as a function of distance, from photoemission imaging and from spatially resolved sonometric recordings. Good agreement is found with numerical simulations. Simulations reveal an important self shortening of the pulse duration, suggesting that laser pulses with few optical cycles could be obtained via double filamentation. An important lowering of the voltage required to induce guided electric discharges between charged electrodes is measured at high laser pulse repetition rate.

OCIS codes: (190.5940) Self-action effects; (140.7090) Ultrafast lasers; (320.2250) Femtosecond phenomena.

References and links

1. A. Giesen, J. Speiser, "Fifteen years of work on thin-disk lasers: results and scaling laws," IEEE J. Sel. Top. Quantum Electron. **13**(3), 598–609 (2007).
2. T. Metzger, A. Schwarz, C. Y. Teisset, D. Sutter, A. Killi, R. Kienberger, and F. Krausz, "High-repetition-rate picosecond pump laser based on a Yb:YAG disk amplifier for optical parametric amplification," Opt. Lett. **34**, 2123-2125 (2009).
3. S. Klingebiel, M. Schultze, C. Y. Teisset, R. Bessing, M. Haefner, S. Prinz, M. Gorjan, D. H. Sutter, K. Michel, H. G. Barros, z. Major, F. Krausz, and T. Metzger, "220 mJ Ultrafast Thin-Disk Regenerative Amplifier," in *CLEO: 2015*, OSA Technical Digest (online) (Optical Society of America, 2015), paper STu4O.2.
4. H. Fattahi, H. G. Barros, M. Gorjan, T. Nubbemeyer, B. Alsaif, C. Y. Teisset, M. Schultze, S. Prinz, M. Haefner, M. Ueffing, A. Alismail, L. Vámos, A. Schwarz, O. Pronin, J. Brons, X. T. Geng, G. Arisholm, M. Ciappina, V. S. Yakovlev, D.-E. Kim, A. M. Azzeer, N. Karpowicz, D. Sutter, Z. Major, T. Metzger, and F. Krausz, "Third-generation femtosecond technology," Optica **1**(1), 45 (2014).
5. A. Couairon, A. Mysyrowicz, "Femtosecond filamention in transparent media," Phys. Rep. **441**, 47-189 (2007).
6. J. Kasparian and J.-P. Wolf, "Physics and applications of atmospheric nonlinear optics and filamentation," Opt. Express **16**, 466–493 (2008).
7. S.L. Chin, *Femtosecond Laser Filamentation* (Springer, 2010).
8. H. M. Milchberg, Y.-H. Chen, Y.-H. Cheng, N. Jhajj, J. P. Palastro, E. W. Rosenthal, S. Varma, J. K. Wahlstrand,and S. Zahedpour, "The Extreme Nonlinear Optics of Gases and Femtosecond Filamentation," Phys. Plasmas **21**,10091 (2014).
9. M. Durand, A. Houard, B. Prade, A. Mysyrowicz, A. Durécu, B. Moreau, D. Fleury, O. Vasseur, H. Borchert, K. Diener, R. Schmitt, F. Théberge, M. Chateauneuf, J.-F. Daigle and J. Dubois, "Kilometer range filamentation," Opt. Express **21**, 26836 (2013).
10. Y.R. Shen, *The Principle of Nonlinear Optics* (Wiley-Interscience, 1984).
11. G. Point, C. Milián, A. Couairon, A. Mysyrowicz, and A. Houard, "Generation of long-lived underdense channels using femtosecond filamentation in air," J. Phys. B **48**, 094009 (2015).
12. E. W. Rosenthal, J. P. Palastro, N. Jhajj, S. Zahedpour, J. K. Wahlstrand and H M Milchberg, "Sensitivity of propagation and energy deposition in femtosecond filamentation to the nonlinear refractive index," J. Phys. B: At. Mol. Opt. Phys. **48**, 094011(2015).
13. J.H. Marburger, "Self-focusing theory," Prog. Quant. Electr. **4**, 35-110 (1975).

14. A. Talebpour, M. Abdel-Fattah, A.D. Bandrauk, and S.L. Chin, “Spectroscopy of the gases interacting with intense femtosecond laser pulses,” Laser Phys. **11**, 68-76 (2001).
15. S. Mitryukovskiy, Y. Liu, P. Ding, A. Houard, A. Couairon, and A. Mysyrowicz, “Plasma luminescence from femtosecond filaments in air: evidence for impact excitation with circularly polarized light pulses,” Phys. Rev. Lett. **114**, 063003 (2015).
16. G. Point. Energy deposition in air from femtosecond laser filamentation for the control of high voltage spark discharges. Optics [physics.optics]. Ecole Polytechnique, 2015. English. <tel-01202982>
17. G. Point, E. Thouin, A. Mysyrowicz, and A. Houard, “Energy deposition from focused terawatt laser pulses in air undergoing multifilamentation,” Opt. Express **24**, 6271 (2016).
18. L.V. Keldysh, “Ionization in the Field of a Strong Electromagnetic Wave,” Zh. Eksp. Teor. Fiz. **47**, 1945 (1964) [Sov. Phys. JETP **20**, 1307 (1965)].
19. K. Lim, M. Durand, M. Baudelet and M. Richardson, “Transition from linear- to nonlinear-focusing regime in filamentation,” Sci. Rep. **4,** 07217 (2014).
20. A. Couairon, E. Brambilla, T. Corti, D. Majus, O. de J. Ramírez-Góngora, M. Kolesik, “Practitioner’s guide to laser pulse propagation models and simulation,” Eur. Phys. J. Spec. Top. **199**, 5-76 (2011).
21. P. Polynkin and M. Kolesik, “Critical power for self-focusing in the case of ultrashort laser pulses,” Phys. Rev. A **87**, 053829 (2013).
22. D. Mikalauskas, A. Dubietis, R. Danielius, “Observation of light filaments induced in air by visible picosecond laser pulse,” Appl. Phys. B **75**, 899–902 (2002).
23. J. Galinis, G. Tamošauskas, I. Gražulevičiūtė, E. Keblytė, V. Jukna, and A. Dubietis, “Filamentation and supercontinuum generation in solid-state dielectric media with picosecond laser pulses,” Phys. Rev. A **92**, 033857 (2015).
24. C.P. Hauri, W. Kornelis, F.W. Helbing, A. Heinrich, A. Couairon, A. Mysyrowicz, J. Biegert , U. Keller, “Generation of intense, carrier-envelope phase-locked few-cycle laser pulses through filamentation,” Appl. Phys. B **79**, 673-677 (2004).
25. D. V. Kartashov, A. V. Kirsanov, A. M. Kiselev, A. N. Stepanov, N. N. Bochkarev, Y. N. Ponomarev, and B. A. Tikhomirov, “Nonlinear absorption of intense femtosecond laser radiation in air,” Opt. Express **14**, 7552–7558 (2006).
26. Y.-H. Cheng, J. K. Wahlstrand, N. Jhajj, and H. M. Milchberg, “The effect of long timescale gas dynamics on femtosecond filamentation,” Opt. Express **21**, 4740-4751 (2013).
27. L. Arantchouk, A. Houard, Y. Brelet, J. Carbonnel, J. Larour, Y-B André and A. Mysyrowicz, “A simple high-voltage high current spark gap with subnanosecond jitter triggered by femtosecond laser filamentation,” Appl. Phys. Lett. **102**, 163502 (2013).
28. E. Schubert, D. Mongin, J. Kasparian, and J.-P. Wolf , “Remote electrical arc suppression by laser filamentation,” Opt. Express **23**, 28640 (2015).
29. A. Schmitt-Sody, D. French, W. White, A. Lucero, W. P. Roach, V. Hasson. “The importance of corona generation and leader formation during laser filament guided discharges in air,” Appl. Phys. Lett. **106**, 124101 (2015).
30. T.-J. Wang, Y. Wei, Y. Liu, N. Chen, Y. Liu, J. Ju, H. Sun, C. Wang, H. Lu, J. Liu, S. L. Chin, R. Li, and Z. Xu “Direct observation of laser guided corona discharges,” Sci. Rep. **5**, 18681 (2015).
31. S. Tzortzakis, B. Prade, M. Franco, A. Mysyrowicz, S. Hüller, and P. Mora, “Femtosecond Laser-guided Electric Discharge in Air,” Phys. Rev. E **64**, 57401 (2001).
32. P. Panagiotopoulos, P. Whalen, M. Kolesik and J. V. Moloney, “Super high power mid-infrared femtosecond light bullet,” Nature Photon. **9**, 543-548 (2015).

1. Introduction

Thanks to the development of diode pumping, laser systems operating at a wavelength close to 1 µm with picosecond pulse duration, peak powers on the order of 10^{11} W and kHz repetition rate are now available [1-3]. Even higher values reaching the TW are expected in the near future [4]. This unavoidably raises the issue of the propagation of such pulses through atmosphere and other transparent media. It is well known that at such high peak powers the pulse propagation is highly nonlinear. Pulses of femtosecond duration undergo filamentation, a process during which a dynamic competition between diffraction, self-focusing, plasma defocusing, and other nonlinear effects lead to the emergence of a beam with narrow diameter and high peak intensity ($10^{13\text{-}14}$ W/cm²) that is maintained over long distances [5-9].

So far most experiments on propagation of short laser pulses in gases have been performed at a wavelength of 800 nm (where reliable fs laser sources based on Ti:Sapphire technology are available). They are well explained by the classical filamentation model where reabsorption of laser energy by the plasma plays a minor role because of the short pulse

duration. On the other hand with intense laser pulses of longer, nanosecond or sub-nanosecond duration, another scenario occurs. Once the critical intensity for ionization is reached on the ascending part of the pulse, the rest of the pulse is reabsorbed by the plasma in an inverse bremhsstrahlung effect, leading to the rapid multiplication of free electrons and dielectric breakdown of the medium. Most of the laser energy is consumed locally at a distance fixed by the moving focus model [10-12].

In this paper we characterize the nonlinear propagation of laser pulses of picosecond duration with a high power high repetition rate diode pumped 1.5 ps laser at 1.03 µm. The manuscript is organized in the following way. First the diode pumped laser characteristics are presented. Then evidence for filamentation is presented. A first qualitative evidence of filamentation is obtained by burn patterns on photographic plates. A collimated pulse emerging from the laser shrinks in diameter and then maintains a narrow beam size over a long distance. With a converging pulse, one observes a shift of the focus towards the laser, followed by the propagation of an intense pulse of reduced diameter persisting well beyond the geometric focus. Direct evidence of high field air ionization is obtained by the observation of a blue emission from the collapsed beam region. From spectral analysis of this emission, formation of a plasma channel is deduced. Laser energy loss in air as a function of incident pulse energy is measured for different laser beam convergences. Laser energy deposition as a function of distance is also measured by a sonometric method. Results are then compared to a simulation assuming the classical filamentation model. The good agreement between experimental results and simulations allows extracting other filament parameters, such as peak intensity, pulse time profile, plasma density and beam diameter as a function of distance. The contribution of inverse bremsstrahlung process to the total density of free electrons is also evaluated. Finally, the triggering of guided electric discharges by the plasma column created in the wake of the filamentary is studied. The role of laser repetition rate on the discharge threshold is analyzed. We draw conclusions on the merit of such a laser for applications such as laser lightning rod or virtual plasma antenna.

2. Description of the laser

The laser used for this study is a chirped-pulse regenerative Yb:YAG thin-disk amplifier from TRUMPF Scientific Lasers, operating at 1030 nm wavelength. Based on the TRUMPF Laser technology [2] allowing high average power and high pulse energies, the laser source delivers 1.5 ps pulses with 100 mJ energy at a repetition rate of 1 kHz, corresponding to an average power of 100 W [3]. In our experiment the beam diameter was 4.2 mm FWHM and it was possible to tune the repetition rate of the laser to 10 Hz, 100 Hz and 2.5 kHz.

3. Experimental evidence for filamentation

The filamentary propagation of an intense and short laser pulse through atmosphere can be divided in three stages. A first stage occurs in the absence of ionization. The propagation of the pulse is ruled by a competition between diffraction and self-focusing due to the optical Kerr effect. If the initial laser peak power exceeds a critical value $P_{cr} = 3.72\ \lambda^2/8\pi n_0 n_2$, where P_{cr} = 5.3 GW for a laser wavelength at λ = 1030 nm, the nonlinear focusing effect always overcomes diffraction so that the beam diameter shrinks with distance and the peak laser intensity increases correspondingly. A second stage begins when the laser intensity becomes high enough to induce high field ionization. This stage, which starts at a distance *z*, where

$$\frac{1}{z} = \frac{1}{z_c} + \frac{1}{f}, \tag{1}$$

with *f* the focal length of the lens and

$$z_c = 0.367 \frac{L_d}{\sqrt{\left(\left(P/P_{cr}\right)^{0.5} - 0.852\right)^2 - 0.0219}}, \tag{2}$$

where $L_d = \pi n_0 D_{FWHM}^2/(\lambda \ln(4))$ is the diffraction length and z_c = 5.5 m for 100 mJ can be viewed as the beginning of filamentation [13]. The presence of ionization leads to a complex restructuring of the pulse time profile. The pulse propagates while maintaining a reduced diameter due to the dynamic competition mainly between self focusing and the defocusing effect due to the plasma, leaving a plasma channel in its wake. Finally, a third stage begins when the pulse peak power falls below P_{cr}. Ionization is now absent; the pulse peak intensity is still very high so that a near equilibrium between diffraction and self focusing is established. Diffraction is prevailing and the beam size slowly increasing with distance (Note that this description does not apply to sharply focused beams).

We have used several techniques to detect the occurrence of filamentation in air from the diode pumped laser. A first, qualitative method consists in evaluating the transverse beam fluence distribution as a function of propagation through the darkening it leaves on photographic plates [9]. Unfortunately, contrary to the case of a laser at 800 nm, no systematic study of the darkening of photographic plates as a function of laser intensity is available at 1.03 µm. Therefore this method can only give a rough estimate of the length of filaments and on threshold conditions for appearance of single and multiple filaments, but no reliable information on the beam diameter.

Table 1. Measurement and calculation of the nonlinear focus position for different focusing conditions.

Focusing	collimated	F = 2 m	F = 1 m	F = 0.5 m
Calculation (Marburger)	7.8	1.6	0.9	0.46
Calculations (numerical)	5.43	1.43	0.83	0.44
Measured (burns)	5	1.7		0.45
Measured (luminescence)		1.5	0.82	0.44
Measured (sonometric)		1.45	0.8	0.43

Filamentation starts around 5 m from the laser output and continues over at least 7 m. Space constraints prevented us to measure burn patterns at longer distances. A multifilament regime is observed with the emergence of at least two filaments in parallel. We note that the situation is similar to that observed with a laser pulse at 800 nm, where multi-filamentation is also observed when $P \geq 10\ P_{cr}$. Burn patterns have been also recorded with converging beams of different pulse energies. The distance at which a narrow beam starts is given in Table 1.

A more direct evidence of filamentation is given by the characteristic blue-UV emission from the plasma. An image of this luminescence track is shown in Fig. 1 for a beam focused with a f = 0.5 m lens. The emission consists in a group of lines around 355 nm. These lines are well documented in the literature as arising from excited nitrogen molecules, both neutral and singly ionized [14-15]. Excitation of nitrogen molecules requires the presence of free electrons. Therefore the luminescence track measures the range over which the intensity in the beam is sufficient for ionization to take place.

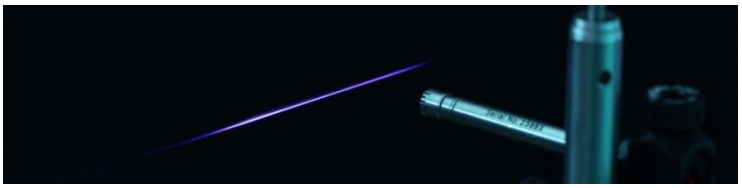

Fig. 1. Photograph of a filament generated luminescence and a microphone to record sound waves The length of the blue emission track is ~ 0.2 m.

Luminescence tracks were investigated by recording their image with a CCD camera. The plasma luminescence track extends to almost half a meter when 100 mJ pulses were focused by 2 m focal lens. A clear displacement of the onset of ionization towards the laser is observed for increasing laser power (see Fig. 2(a)). Although it provides direct evidence for a

plasma column, this technique does not measure precisely its length and position because of image distortion by the objective of the camera due to the length of the column (~ 50 cm).

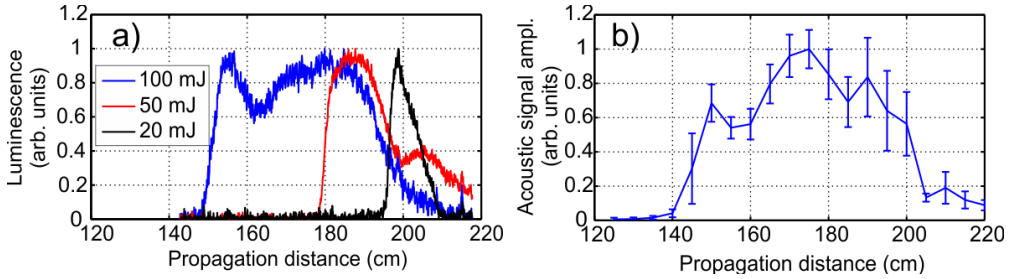

Fig. 2. Luminescence power (a) and acoustic signal amplitude (b) recorded for beam focused with 2 m focal length lens. Acoustic signal ampliture was recorded for 100 mJ energy pulse and with a repetition rate of 1 kHz.

Another technique is sonometric. By displacing a microphone (model 40BE from G.R.A.S. with a 4 Hz-100 kHz bandwidth) along the plasma column, it is possible to measure the lineic energy deposition of the laser pulse during propagation [16-17]. The sound wave maximum amplitude is plotted in Fig. 2(b) as a function of propagation distance for a 100 mJ pulse energy laser beam focused with a 2 m lens.

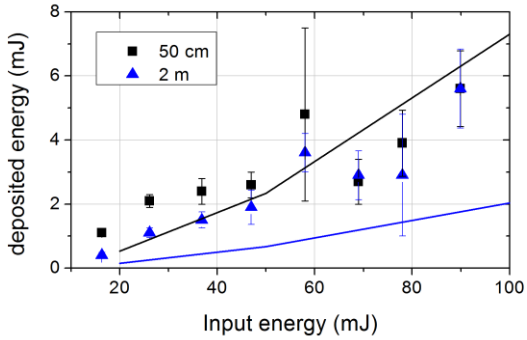

Fig. 3. Deposited energy dependence on input energy measured for two focal lengths (dots) with a repetition rate of 1 kHz. Continuous lines show the calculated deposited energy for similar conditions.

We have also measured the energy deposited in air during propagation of laser pulses with different convergences by measuring with a powermeter the transmitted versus input laser energy. Results are shown in Fig. 3. The deposited laser energy loss increases monotonically with input laser energy and amounts to ~ 5 % at our highest laser powers.

4. Simulations

We have performed numerical simulations of the propagation of laser pulses with characteristics close to those of the experiment. An initial beam with Gaussian profile of 4.2 mm diameter FWHM was adopted. The initial laser beam spatial profile had a small ellipticity which is ignored in our cylindrical symmetry code (it is assumed that this ellipticity has only a small effect on the focused beam nonlinear dynamics). Otherwise all laser parameters are those given in section 2.

The propagation equation for pulse envelope written in Fourier domain is the following:

$$\partial_z E_{k_x,k_y}(\omega,z) = iK_{\omega_0}(\omega,k_x,k_y)E_{k_x,k_y}(\omega,z) + \frac{i}{2\varepsilon_0 c^2 \kappa_{\omega_0}(\omega)}[\omega P_{k_x,k_y}(\omega,z) + iJ_{k_x,k_y}(\omega,z)], \qquad (3)$$

where

$$K_{\omega_0}(\omega,k_x,k_y)=k(\omega)-\kappa_{\omega_0}(\omega)-\frac{k_\perp^2}{2\kappa_{\omega_0}(\omega)},\ \text{and}\ \kappa_{\omega_0}(\omega)=k_{\omega_0}+k'_{\omega_0}(\omega-\omega_0). \tag{4}$$

w,$k_\perp$ are Fourier space variable variables. The first term describes linear effects while the second term – nonlinear effects. P and J are nonlinear polarization and current:

$$P(\tau,r,z)=2n_0n_2\varepsilon_0\left\{(1-\alpha)|E|^2E+\alpha\left[\int_{-\infty}^{t}R(t-t')|E(t')|dt'\right]E\right\}, \tag{5}$$

$$R(t)=R_0\exp(-\Gamma t)\sin(\omega_r t), \tag{6}$$

$$J(\tau,r,z)=c\sigma\varepsilon_0(1+i\omega_0\tau_c)\rho E+cn_0\varepsilon_0\frac{W(I)K\hbar\omega_0}{I}\left(1-\frac{\rho}{\rho_{nt}}\right)E. \tag{7}$$

Plasma density was calculated using this relation:

$$\frac{\partial\rho}{\partial t}=W(I)(\rho_{nt}-\rho)+\frac{\sigma}{U_i}\rho I\ , \tag{8}$$

where n_0 is refractive index, $k(\omega)$ is wavenumber, n_2 is nonlinear refractive index, α is repartitioning factor for delayed Raman Kerr effect, Γ and ω_r are molecular response parameters for delayed Raman Kerr effect, $R_0 = (\Gamma^2+\omega_r^2)/\omega_r$, τ_c is electron collision time, ρ_{nt} is density of neutrals, K is multiphoton ionization order, U_i is air bandgap, and $W(I)$ is the full Keldysh ionization rate [18]. All material parameters used in this study were taken from [19] while the numerical scheme has been taken from [20].

5. Comparison with experimental results and discussion

Table 1 summarizes the measured distance for the onset of filamentation measured with the different techniques under various laser conditions and gives a comparison with the distance derived from the Marburger formula (Eq. (1)). There is a good overall agreement except that Eq. (1) predicts a larger shift than observed. We note in this respect that the Marburger formula is strictly valid for a CW laser beam of Gaussian spatial profile and therefore gives only a rough estimate of the distance for the onset of filamentation [21]. The onset of filamentation from the full numerical simulations shows better agreement with experimental results. To compare plasma luminescence tracks with simulations, we have integrated the calculated plasma density over the radial coordinate and assumed that the luminescence is linearly proportional to the plasma density. Numerical results for three different pulse powers are presented in Fig. 4(a). The shape of the luminescence power is similar to the numerical plots. The position of the experimentally recorded luminescence tracks are in fair agreement with numerical data, although a small shift probably comes from a slightly defocusing input beam. In the numerical data graphs, we also plot the free electron plasma contribution due to the avalanche process. As can be seen, electrons produced by inverse bremsstrahlung represent around 20% of the total plasma density. For comparison, simulations performed with a 100 fs laser pulse of comparable peak intensity, the contribution to plasma density from avalanche multiplication amounts to 3-5 %. We have also calculated that the losses due to molecular rotation only amount to 5.5% of total losses in our case, while it can exceed 50% in the case of 130 fs pulse at 800 nm [12]. The use of the long pulse duration strongly decreases the losses due to Raman Effect.

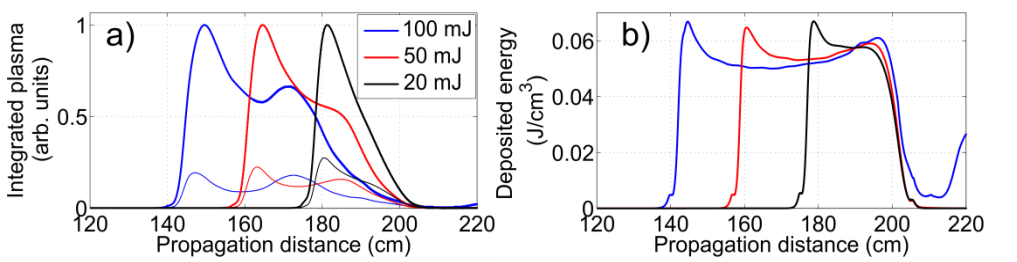

Fig. 4. Simulation results showing integrated plasma density over the radial coordinate (equivalent to plasma luminescence power) (a) and maximum reached plasma density (b) as a function of propagation distance and for different initial pulse energies. A 2 m focal length lens was used to focus the beam. The thin lines in subfigure (a) give the contribution to the plasma from inverse bremsstrahlung.

In order to compare the results of sonometric detection with simulations, we assume that the initial pressure profile of the acoustic wave produced by filamentation is linearly proportional to the amount of deposited energy. As shown before, most of the energy of the pulse is lost through ionization process. We also assume that the sound wave propagates without distortions up to the microphone set at 2 cm from the plasma column. Under these assumptions we compare the calculated maximum of deposited energy over the propagation distance with the experimentally acquired acoustic signal. Figure 4(b) shows the comparison for a laser beam focused by 2 m lens. There is a good agreement between experimental acoustic signals and numerical simulations of maximum plasma density, as can be seen by comparing Figs. 2(b) and 4(b). Finally, calculated total energy loss versus input laser energy are consistent with the experimental results as shown in Fig. 3.

The good agreement between experiments and simulations validates the propagation code and allow extracting other features of the laser pulse during filamentation. We concentrate on the case of a laser beam focused by a 2 m lens. In Fig. 5, the beam diameter at half maximum intensity is plotted as a function of propagation distance. Up to 80 cm of propagation, the beam size does not differ significantly from a linear case. Beam self-focusing becomes apparent upon further propagation until the beam starts to collapse around 140 cm. Ionization occurring at that stage leads to a defocusing followed by a refocusing until the beam size finds a quasi equilibrium after 200 cm, with a beam of nearly constant diameter.

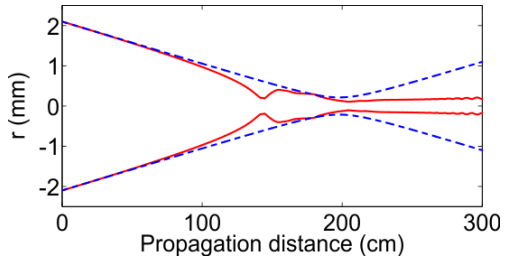

Fig. 5. Beam profile as a function of propagation distance. Shown is the diameter of the beam (FWHM) (red curve) in the nonlinear regime and the corresponding diameter in a linear propagation regime (blue dotted curve).

Figure 6 represents the axial pulse intensity evolution during propagation through atmosphere. The laser pulse with 1.5 ps initial duration (FWHM) propagates without strong alteration up to 130 cm because the peak intensity is still relatively small and the propagation length is not sufficient to accumulate a significant nonlinear phase shift. Upon further propagation the pulse experiences a symmetric self compression due to nonlinear self-focusing up to 142 cm. The pulse intensity then increases rapidly until plasma is generated. It reaches a saturated value $I \sim 2.3 \times 10^{13}$ W/cm². Reabsorption of pulse energy by the plasma and defocusing occurs at the rear part of the pulse. The energy to sustain large losses at the beam

center comes from the geometrical focusing of the beam. Therefore the pulse constantly generates plasma and shifts its maximum position. As a consequence, the peak travels at superluminal speed, while further shrinking in time. The pulse duration at 170 cm becomes 157 fs (FWHM). Note that pulse self-shortening of a picosecond laser pulse at 527 nm has been previously reported in [22]. This dynamics is visible up to the focus of the lens. After the linear focus of the lens, laser pulse energy reappears at the initial center of the beam, leading to the generation of multiple peaks. A pulse peak at the center is restored due to self-focusing, geometric focusing from initial beam parts less affected by plasma defocusing, but also from linear beam transformations like diffraction and Arago spot generation. As shown by Galinis *et al.*, this new born central peak can produce supercontinuum [23]. The evolution of the pulse at different stages is depicted in Figs. 6(b) and 6(c). The calculated pulse dynamics suggests that it should be possible to reduce the pulse duration further by using a double filamentation sequence similar to that of Hauri *et al.* [24]. Indeed, according to our simulation, a pulse of 150 fs pulse duration at 1.03 µm focused by a 2 m lens shortens to a duration of 30 fs.

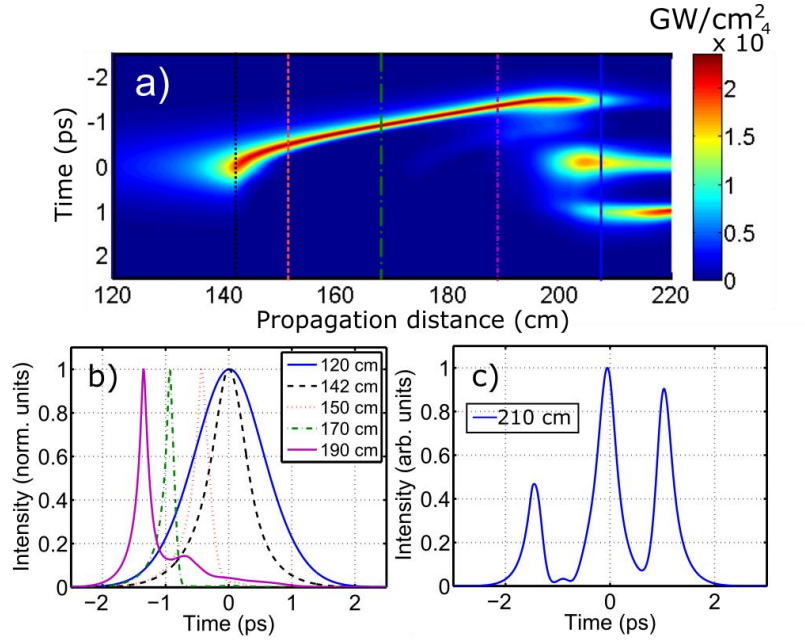

Fig. 6. Axial pulse intensity dependence on propagation distance (a). 100 mJ pulse was focused by 2 m lens. Also shown is the pulse time profile at different propagation distances (b and c).

The on-axis laser spectrum has been measured after the end of the filament and compared to the calculated spectrum at a distance of 220 cm, considering an aperture of 10 µm. Both experimental and calculted spectra display significant broadening as shown in Fig. 7. We note that the spectral broadening of the transmitted pulse is consistent with the self-shortening effect previously described. The transform limited pulse corresponding to the experimental spectrum gives a pulse duration of 164 fs FWHM, in very good agreement with the calcultions.

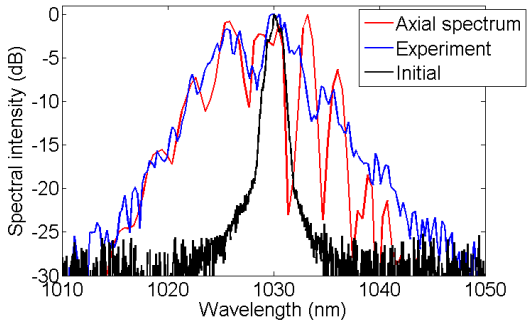

Fig. 7. Measured laser spectrum before (black curve) and after filamentation (blue curve) and calculated output axial spectrum at a distance of 220 cm (red curve).

Having described the pulse transformation process we now examine the beam transformation dynamics. In Fig. 8, we plot the beam fluence dependence on propagation distance. All transformations of beam fluence profiles can be tracked by connecting each reshaping of the pulse intensity profile to a corresponding reshaping of the fluence profile. Up to 142 cm there is only beam focusing and self-focusing. From 142 cm on, the beam generates plasma which rapidly defocuses the beam center where most of the plasma is generated. The defocusing of the center of the beam together with the focusing due to linear beam propagation transforms the fluence profile to a ring shaped structure. The fluence profile dependence on propagation distance over this region takes the "<" shape of a diverging ring. At the center of the beam, the pulse shortens, energy gets lower, but intensity is still high enough to generate plasma. Later in propagation, linear focusing starts to play the major role and generates a ">" shaped converging ring. There is still a lot of laser energy outside the center portion of the beam. It continues to squeeze itself up to the linear focus. At the end of the propagation (2.2 m) we see that the fluence of the beam is composed of two parts. At the center of the beam fluence peak appears, while further away from the center we notice the beam energy part which was defocused by the plasma and forms a background or energy reservoir.

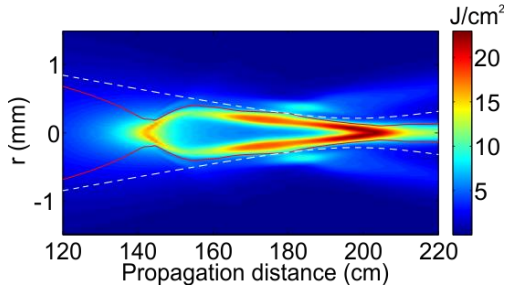

Fig. 8. Beam fluence as a function of propagation distance for a 100 mJ energy pulse focused by 2 m focal length lens.

Occurrence of a ring structure of the pulse fluence does not mean that the plasma density or the deposited energy is smaller at the center of the beam. The dependence of these quantities on propagation distance is depicted in Fig. 9. The densest plasma is in the regions where the beam fluence was pushed outwards from the center. Deposited energy plots show areas of energy loss. It is directly connected to plasma density because the plasma recombination rate can be neglected during the pulse duration.

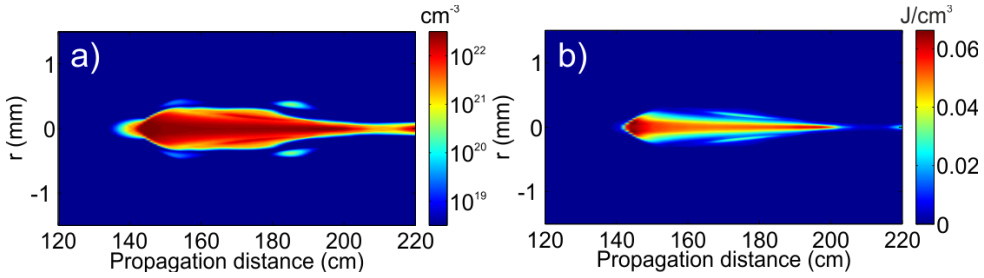

Fig. 9. Energy deposition and plasma density dependence on propagation distance for a 100 mJ energy pulse focused by 2 m focal length lens.

To estimate the influence of laser wavelength and pulse duration on the filamentation process we performed simulations at 800 nm with an imput pulse duration of 1.5 ps and 100 fs with similar input beam parameters. We considered propagation in air of a Gaussian laser pulse with a peak power of 66 GW and a diameter of 4.2 mm FWHM focused by a f = 2 m converging lens. In Table 2 the calculated loss repartition is given for the three sets of laser parameters considered. The evolution of the absorbed energy and integrated plasma density as a function of the propagation distance is also presented in Fig. 10.

Table 2. Calculated energy losses during filamentation for different laser wavelengths and pulse durations for a constant laser peak power of 66 GW.

	Wavelength	Duration	Input energy	Total energy losses	Loss repartition		
					Avalanche absorption	Raman absorption	Multiphoton ionization
Pulse 1	1032 nm	1.5 ps	100 mJ	**2 %**	20%	4.6%	75.4%
Pulse 2	800 nm	1.5 ps	100 mJ	**3.5 %**	12%	3.3%	84.7%
Pulse 3	800 nm	100 fs	6.6 mJ	**20 %**	2.3%	6.3%	91.4%

Comparing the picosecond pulses at 1032 nm and 800 nm, on can see that there is a transfer of loss mechanisms from multiphoton ionization to avalanche absorption as the wavelength is increased. However this is not significant enough to alter the classical scenario of filamentation. The pulse duration seems to have a stronger influence on the energy losses. By decreasing the pulse duration to 100 fs, Raman absorption becomes significant (as observed in [12,25]) and multiphoton ionization is strongly increased. The total energy losses are then raised to 20%. This effect of the pulse duration on energy deposition should have an impact on the hydrodynamic evolution of the filament, but it doesn't seem to affect significantly the filament length and plasma density as shown by Fig. 10.

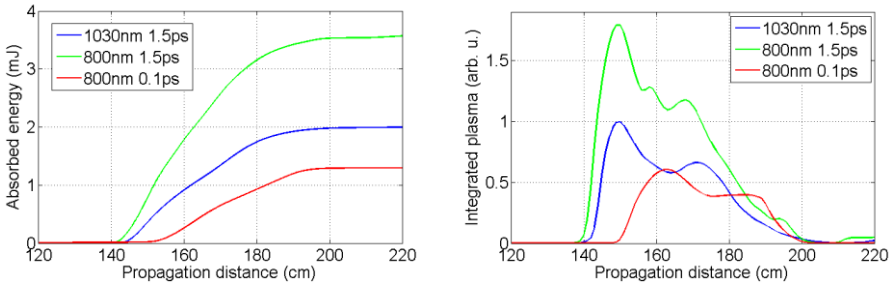

Fig. 10. Calculated absorbed energy (a) and integrated plasma density (b) as a function of propagation distance for a laser pulse focused in air by a 2 m focal length lens with an input diameter of 4.2 mm FWHM. Blue curves correspond to a pulse at 1032 nm, with duration 1.5 ps and 100 mJ of energy. Green curve: 800 nm, 1.5 ps and 100 mJ. Red curve: 800 nm, 100 fs and energy of 6.6 mJ.

Finally, we address the problem of the generated modification in atmospheric gas profiles after the passage of the pulse. It has been recently shown with laser pulses at 800 nm

that the energy deposited by filamentation gives rise to a long-lasting column of density depression [26,11,17]. Such low density channels offer a preferential path for electric discharges. Since the depression can reach ms, one can then expect a significant change of threshold conditions for triggering a guided electric discharge at kHz repetition rate.

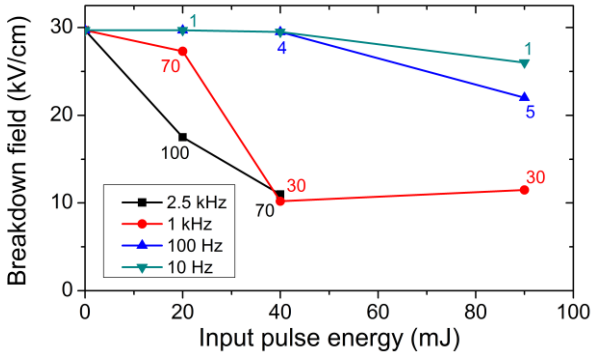

Fig. 11. Breakdown field dependence on laser pulse energy measured for different repetition rates. For each measurement the average number of laser shots necessary to obtain the breakdown is also indicated.

Figure 11 validates this expectation. The threshold for electric breakdown between two plane electrodes separated by 10 mm is measured when a DC voltage is applied. A central hole drilled in the electrodes allows the laser filament to cross the gap (see description of the spark gap electrode in [27]). The laser is focused with a lens of 1 m focal, and the spark gap is placed at 95 cm from the focusing lens. In the absence of a laser pulse, an electric field of 29.7 kV/cm is required for spontaneous breakdown. When the laser is turned on, an important reduction of the breakdown field is observed, especially at high repetition rate. As shown in Fig. 11 the threshold for laser discharge is reduced by a factor 3 going from a 10 Hz to kHz repetition rate. For the laser working at a repetition rate of 10 Hz, the breakdown always occured a few tens of ns after the first laser pulse is send. At higher repetition rate, guided discharges could be obtained at a lower voltage, but in this case the breakdown appears afer several tens of laser pulse have been send. The average number of laser shots necessary to obtain the breakdown is indicated in Fig. 11 for each set of parameter. This tends to show that the lowering of the breakdown voltage associated with the laser repetition rate is a cumulative effect, similar to the one observed by Cheng. *et al.* who measured the hydrodynamic evolution of filament generated in air at 1 kHz [26].

We note that the observed dependence of the discharge process from the laser repetition rate may also be relevant for the remote neutralisation effect recently reported by Schubert *et al.* with a 15 mJ femtosecond laser at 800 nm [28]. They observed a suppression of the electric arc produced between two spherical electrodes when filaments were generated at 1 kHz in the vicinity of the electrodes. The difference might be explained by the fact that they use a vey non-uniform electric field due to the shape of the electrodes and the gap length (12 cm). This favors the development of coronas, which tends to decrease the breakdown voltage and seems to be sensitive to the plasma produced by filaments [28,29,30]. In our case, with a quasi uniform field, the triggering effect appears to be purely related with hydrodynamic effect produced by the filament as described in [31].

6. Conclusions

We have characterized the propagation in air of laser pulses of 100 GW peak power and ps pulse duration. Evidence of filamentation and plasma formation has been reported based on several detection techniques. A detailed comparison between experimental results and simulations using the classical filamentation model was done when the laser beam was focused with a 2 m lens. Good overall agreement between experiments and simulations was

found. This shows that the classical filamentation model is applicable to laser pulses around 1 µm (a recent theoretical publication shows that with mid IR laser pulses, a different filamentation process occurs where plasma formation does not play a major role anymore [32]). Since simulations here pertain to a single isolated laser pulse, there is no obvious effect of the high laser repetition rate on the pulse evolution during propagation, at least for this 2 m converging geometry. Drawing on numerical results, we show that, in the region where multiphoton ionization occurs, the pulse propagates at superluminal speed and experiences pulse splitting and an important self shortening, with the pulse duration reducing to a minimum value of ~ 157 fs. This suggests that it should be possible to obtain even shorter, few cycle optical pulses by using a configuration similar to that of Hauri *et al.* at 800 nm [24]. The contribution of free electron production by an avalanche process has been estimated. It is significantly higher than with sub-picosecond laser pulses but still does not prevent the major part of the initial laser energy to propagate well beyond the focused region. Finally, we found an important reduction of the voltage necessary to obtain a guided discharge induced by filamentation at high repetition rate. This, together with the fact that extended plasma columns are formed shows that diode pumped lasers are good candidates for establishing a lightning rod in the sky.

Acknowledgments

The authors thank Jérôme Carbonnel, Leonid Arantchouk and Nicolas Baudet for technical assistance, and acknowledge financial support from the french DGA (grants No 2013.95.0901, No 2012.60.0011 and No 2012.60.0013).